Intraseasonal dependence, wave energy accumulation and the formation of intense South Atlantic Convergence Zones

Fernando E. Hirata[1] and Peter J. Webster[1]

[1] Department of Physics, Universidade Federal do Paraná, Brazil

[2] School of Earth and Atmospheric Sciences, Georgia Institute of Technology, Georgia, USA.

Corresponding author: F.E. Hirata, Department of Physics, Universidade Federal do Paraná, Brazil (fernando.hirata@eas.gatech.edu).

Keywords: South Atlantic Convergence Zone, intraseasonal variability, wave accumulation

Abstract

Intense South Atlantic Convergence Zone (SACZ) events are linked to the Madden-Julian oscillation (MJO) life cycle and to the accumulation of synoptic wave energy in a region of upper-level negative zonal stretching deformation off eastern Brazil. These events correspond to 20% of all identified SACZs from 1979 to 2011 and occurred before MJO initiation over the Indian Ocean. However, the intraseasonal precursors of intense SACZ are related to the previous transition from active to break convective phases over the Maritime Continent. Intraseasonal convection in the SPCZ region, not necessarily associated with preceding MJO convection, is observed to the east of the MJO convective break. An upper-level extratropical wave train is propagates from the SPCZ region to South America. High frequency (3-6-day) systems become more frequent and propagate equatorward along the eastern Brazilian coast until a region of climatological negative zonal stretching deformation. The zonal deceleration of upper-level winds is associated with seasonal changes in the subtropical jet stream driven by the establishment of the South American summer monsoon. The negative zonal stretching deformation decreases synoptic disturbances longitudinal extent and propagation speed, increases wave energy density and intensifies the SACZ convective activity.

1. Introduction

The South Atlantic Convergence Zone (SACZ) is the most prominent feature of summertime intraseasonal variability over South America. It is usually defined as a band of deep convection oriented from northwest to southeast, extending from the Amazon basin into the South Atlantic Ocean with a varying spectral structure along its axis (Figure 1). Close to the equator, intraseasonal and synoptic variations are less energetic. To the southeast, intraseasonal variability peaks over the Brazilian coast south of 12^{o}S and synoptic disturbances are relatively more important in the subtropics over the ocean. The spectral structure and orientation of the SACZ strongly resembles features observed in the South Pacific Convergence Zone (SPCZ) [Widlansky et al., 2010].

The association of a subtropical convergence zone with a monsoonal circulation is commonly observed worldwide. Moisture convergence and abundant rainfall near the boundary between an upper-level high pressure system generated by the monsoon and subtropical jet streams occur in the SPCZ, the SACZ, and in the Baiu frontal zone in Asia [Kodama, 1992]. In South America, the establishment of the summer monsoon has been suggested to be a fundamental for the first SACZ of the season [Ferreira et al., 2011], which occurs after a change in behavior of propagating synoptic cyclonic disturbances forced by the development of a summertime upper-level high pressure center over the continent (Bolivian High). The seasonal formation of the Bolivian High, driven mostly by Amazon convection [Lenters and Cook, 1997], alters the upper-level wind field (Figure 1c), enhancing anticyclonic shear in the northern flank of the subtropical

jet. The horizontal shear would force transient extratropical disturbances to thin and tilt westward, promoting the diagonal orientation of the first SACZ [Ferreira et al., 2011].

The influence of the Bolivian High on upper-level winds also deepens the negative zonal stretching deformation (200 mb $\partial \bar{U}/\partial x < 0$) over south and eastern Brazil (Figure 1c), in a region that coincides with the SACZ climatological position (Figure 1a). In the Pacific, the location and orientation of the SPCZ is determined by the location of a region of negative zonal stretching deformation, which is set up by the zonal SST gradient across the South Pacific basin [Widlansky et al., 2010]. Webster and Chang, [1997] derived two expressions relating the zonal stretching deformation to longitudinal wavenumber (k) and wave energy density (ξ) when the background wind field varies gradually in space and the frequency of synoptic-scale Rossby waves is conserved:

$$\frac{dk}{dt} = -k\frac{\partial \bar{U}}{\partial x}$$

$$\frac{d\xi}{dt} = -\xi\frac{\partial \bar{U}}{\partial x}$$

Negative zonal stretching deformation increases the longitudinal wavenumber of synoptic Rossby waves propagating eastward (which leads to a reduction of the longitudinal group speed) and increases wave energy density. The local increase of wave energy density (*wave accumulation*) results in intense convective activity that forms the diagonal band of low outgoing longwave radiation (OLR) characteristic of the SPCZ [Widlansky et al., 2010]. Similarities between the background summertime conditions in the SPCZ and the SACZ lead to the hypothesis that wave energy accumulation also plays a role in the SACZ dynamics.

The location, orientation, and persistence of subtropical convergence zones require a physical mechanism to sustain strong stationary convection and heavy rainfall for a few days. In theory, wave energy accumulation and horizontal anticyclonic shear arguments are not exclusives. The two mechanisms may act in concert to generate the observed characteristics of subtropical convergence zones because both are associated with changes of the subtropical jet by the seasonal growth of an upper-level anticyclone. The climatological regions of summertime negative zonal stretching deformation and anticyclonic horizontal shear in the surroundings of Southern Hemisphere subtropical convergence zones coincide because both are associated with the subtropical jet. Nonetheless, wave energy accumulation arguments are able to address location, orientation, and persistence of subtropical convergence zones, indicating that a certain level of accumulated energy must be acquired from one or more propagating disturbances before the convergence zone event is triggered.

As it can be observed in Figure 1, the SACZ presents important submonthly (2-30-day) and intraseasonal (30-90-day) variations. Extensive research has focused on the influence of the Madden-Julian Oscillation (MJO) on SACZ variability. The basic idea about the MJO influence over South American convection is that there is a tropical longitudinal connection and a tropical-extratropical connection. The tropical connection is directly tied to the MJO and is characterized by a northward expansion of precipitation over tropical Brazil [Souza and Ambrizzi, 2006] and a more persistent SACZ [Carvalho et al., 2004]. The tropical-extratropical connection represents the influence of extratropical wave activity on both synoptic [Liebmann et al. 1999] and intraseasonal frequencies [Grimm and Silva Dias, 1995]. The SACZ would develop whenever the synoptic and the intraseasonal frequencies become in phase [Cunningham and Cavalcanti,

2006]. Liebmann et al. [1999] argued that extratropical systems act to tap moisture flowing southward from the Amazon and are, therefore, a vital mechanism for SACZ variability.

Extratropical wave activity has been suggested to link variations of the SPCZ with the SACZ on both intraseasonal and interannual time scales. A divergent forcing (heating) southeastward of the SPCZ climatological position, consistent with that imposed by the MJO or the El Niño-Southern Oscillation (ENSO), is able to trigger a barotropic wave train that enhances the SACZ approximately 5 days later [Grimm and Silva Dias, 1995]. Statistically, when convection is suppressed over the Maritime Continent, SACZ events tend to persist for a longer period of time [Carvalho et al., 2004]. Furthermore, intense and long-lived SACZ events are closely related to excessive precipitation over southeastern Brazil [Carvalho et al., 2002]. Hence, an investigation of the mechanisms linking the MJO and the SACZ may extend the range of predictability of extreme rainfall and floods in a heavily inhabited region.

Our goal is to demonstrate that a region of upper-level negative zonal stretching deformation over the eastern coast of Brazil acts to accumulate wave energy, resulting in the occurrence of strong SACZ events. These intense events represent nearly 20% of all identified SACZs. Accumulation of high frequency energy provided by synoptic disturbances is particularly important for SACZs associated with intraseasonal convection over the Eastern Hemisphere. Intraseasonal convective activity in the surroundings of the SPCZ is observed around 10 days before the initiation of a strong and long lasting SACZ. Intense SACZ events tend to precede the initiation of MJO events over the Indian and West Pacific Oceans but their intraseasonal precursors are intimately related to the MJO cycle. On the other hand, most of the identified SACZ events (62%) showed weaker convective anomalies and lack of significant connections with the global intraseasonal cycle. Although MJO-related signals are able to modulate SACZ

intensity and persistence, the origin of these independent SACZ are still unclear and, therefore, independent events are assumed to be less predictable.

The next section introduces the dataset and basic statistical tools used throughout the paper. Section 3 objectively defines the SACZ using Empirical Orthogonal Function analysis (EOF). Section 4 addresses the connection between the SACZ and other major modes of tropical intraseasonal variability. Section 5 presents composite life cycles of SACZ events associated with MJO events and of independent SACZ events. Section 6 highlights the importance of wave accumulation processes for MJO-dependent SACZ events followed by a summary and discussion of the main findings.

2. Data and methods

The dataset used in this study comprises NOAA's OLR [Liebmann and Smith, 1996], CPC unified gauge-station rainfall [Chen et al., 2008] and ERA-Interim reanalysis variables sampled daily from 1979 to 2011. The analyses focus on the austral summer season (October to March). Time series filtering uses a Lanczos-cosine filter with 241 weights in two bands: synoptic (3-6 days) and intraseasonal (20-90 days). Significance at 95% level is assessed through a Monte Carlo technique [Livezey and Chen, 1983].

3. Definition of the SACZ

The SACZ is defined as the first EOF of intraseasonally-filtered OLR over South America (hereafter referred to simply as SACZ). This first mode is not significantly affected by the variations in domain size. Unlike intraseasonal EOF modes of the Eastern Hemisphere tropics, the first two South American patterns depicted by EOF decomposition are not significantly

132 correlated at intraseasonal time scales. The use of North's rule of thumb [North et al., 1982]
133 indicates that only the first EOF can be completely separated from the other modes.

134 The SACZ mode explains 41% of the intraseasonal variance and depicts a dipole-like
135 structure along the Brazilian coast within a region of summertime OLR minimum (Figure 1a).
136 To confirm the close similarity between this statistical pattern and the dynamical structure of the
137 SACZ, a composite cycle is calculated based on SACZ principal component time series
138 (hereafter referred to as SACZ-PC1, Figure 1b). In this composite cycle, day 0 refers to SACZ-
139 PC1 maxima exceeding +1 standard deviation. A total of 106 SACZ events are identified using
140 this definition.

141 The horizontal structure of SACZ events is displayed on Figure 1b using daily rainfall, 850
142 hPa winds, and 500 hPa omega regressed onto the calculated SACZ composite cycle. Significant
143 positive rainfall and negative omega anomalies coincide with the region of negative OLR
144 anomalies depicted by the SACZ mode. The predominance of low-level westerlies north of 15^{o}S
145 associated with a cyclonic flow centered to the south resembles an active phase of the South
146 American monsoon [Jones and Carvalho, 2002]. Negative rainfall anomalies are observed over
147 southern Brazil and Uruguay and this dipole matches the see-saw pattern of relatively dry
148 subtropical plains concurrent with an active SACZ [Nogués-Paegle and Mo, 1997; Carvalho et
149 al. 2004]. The dipole is also consistent with SACZ intraseasonal, interannual and interdecadal
150 variations [Nogués-Paegle et al., 2000; Robertson and Mechoso, 2000]. Therefore, we conclude
151 that the statistical SACZ mode depicts the main characteristics of the SACZ discussed in the
152 literature and we use SACZ-PC1 as an index for SACZ intraseasonal variability.

153 **4. SACZ correlation with main modes of tropical intraseasonal variability**

There are distinct categories of tropical intraseasonal oscillation over the Indian Ocean, Maritime Continent, and West Pacific defined based on the combined evolution of the first and second EOF modes of intraseasonal OLR over the Eastern Hemisphere tropics (hereafter referred to as TEOF1 and TEOF2, Figure 2a,b) [Hirata et al., 2013]. The main category comprises MJO events, with the two remaining categories representing intraseasonal convective events decaying or intensifying to the east of the Indian Ocean (referred to as *eastward decaying* and *eastward intensifying* events, respectively).

Lag correlations between SACZ-PC1 and the principal component time series of T-EOF1 (T-PC1) and T-EOF2 (T-PC2) indicate that the best significant relationship is between the T-PC2 and the SACZ-PC1 (-0.37 with the SACZ-PC1 leading T-PC2 by 1 day, Figure 2c). This association is depicted by T-EOF2 spatial pattern (Figure 2b). Furthermore, T-PC1 and the SACZ-PC1 exhibit significant negative correlation at lag +8 (T-PC1 leads SACZ-PC1). These correlations indicate the traditional association between tropical intraseasonal oscillations and the SACZ: active (inactive) convection over the Maritime Continent is concurrent with a break (active) phase in SACZ convective activity [Carvalho et al., 2004]. It is also worth noting the positive correlation at lag -12 with the SACZ-PC1 leading T-PC1. This correlation suggests that SACZ activity can feedback into the intraseasonal convection cycle over the Eastern Hemisphere.

Tropical intraseasonal oscillation events can be used to determine whether a SACZ event occurred within their life cycles or not, indicating possible connections between each of these distinct intraseasonal categories and the SACZ. Table 1 summarizes the findings of this procedure. The number of SACZ events is much higher than the combined number of intraseasonal events identified by Hirata et al. [2013], suggesting that SACZ occurrences are not

177 influenced only by intraseasonal convection over the Eastern Hemisphere warm pool. Overall,
178 the SACZ seems to be more important for warm pool intraseasonal activity than the other way
179 around: the number of SACZ preceding MJO events (21) is larger than the number of MJO
180 events preceding the SACZ formation (9). In addition, most of the time a SACZ is observed
181 independent of any type of intraseasonal event in the Indian or West Pacific (64 events).

182 **5. Composite life cycles of MJO-dependent and independent SACZ events**

183 In this section, we explore two situations highlighted on Table 1: (1) SACZ preceding MJO
184 events and (2) SACZ independent of the MJO.

185 *5.1 SACZ preceding MJO events (MJO-dependent)*

186 The composite life cycle of tropical convection calculated for the events in which the SACZ
187 leads the MJO (Figure 3) reaffirms the relationships indicated by the lag correlations. When the
188 SACZ-PC1 reaches a maximum above 1 standard deviation (composite day 0 – Figure 3c),
189 convection is active over the SACZ region (although not maximum) while suppressed conditions
190 are observed over the Maritime Continent. Surface pressure anomalies indicate the same pattern
191 associated with a Kelvin-Rossby wave pair discussed by Hirata et al. [2013]. The mismatch of
192 maximum intraseasonal convection and composite day 0 comes from the fact that this category
193 of SACZ events is a subsample of all SACZ events. Independent SACZ composites present a
194 similar behavior, but an average composite cycle of all 106 identified SACZ events does match
195 maximum intraseasonal convection with composite day 0 (not shown).

196 The evolution of OLR anomalies before composite day 0 shows convective anomalies around
197 the SPCZ region, with some activity east of the dateline. At lower levels, negative surface
198 pressure anomalies south of convective anomalies over the tropical West Pacific assume a

northwest-southeast orientation near the dateline at composite day -10 (Figure 3a,b). This set up is resembles an active SPCZ. The negative pressure anomalies off the equator from days -10 to -5 resemble Rossby waves (Figure 3a,b). In this sense, the composite cycle based on SACZ events preceding MJO convection is very similar to the traditional MJO life cycle around the tropics [e.g. Matthews, 2000].

Peak convection over South America and the adjacent South Atlantic Ocean occurs at composite day +5 (Figure 3d), with OLR anomalies comparable in magnitude to the ones observed over the Indian Ocean a few days later (Figure 3e). Maximum convective anomalies over the Indian Ocean are strong after an intense SACZ, indicating again that the relationship between the MJO and the SACZ still holds: convective breaks over the Maritime Continent are observed while convection grows over South America and around two weeks later, the MJO experiences an active phase. This description evidences the dependency of intense SACZ events on the MJO life cycle.

Upper-level geopotential anomalies indicate that extratropical waves linking the Pacific to the Atlantic are important to intensify the SACZ (Figure 4). At day -5, a wave train is clearly organized between Tasmania and southern South America (Figure 4b). After SACZ convection is triggered at composite day 0, a dipole of negative geopotential anomalies around 30^{o}S and positive anomalies just north of 60^{o}S to the east of the South American continent is strengthened until day +5 (Figure 4c,d). The 200 mb geopotential composites are very similar to streamfunction anomalies for pentad lag zero of an intraseasonal event over the warm pool identified on 3 January 1986 [Hsu et al. 1990; Berbery and Nogués-Paegle, 1993]. Hsu et al. [1990] reported that the wave pattern established over the entire Northern Hemisphere could be traced back to the tropical West Pacific on 19 December 1985 associated with convective

222 activity. Berbery and Nógues-Paegle [1993] showed that another wave pattern was excited in the
223 Southern Hemisphere, driven by the same intraseasonal forcing over the Maritime Continent.

224 In our analysis, one of the SACZ events preceding an MJO was identified on 25 December
225 1985. Thus, the extratropical wave pattern along the Southern Hemisphere observed on 19
226 December matches the upper-level geopotential pattern at composite day -5 (which would
227 correspond to 20 December). In fact, 11-day mean vertically integrated diabatic heating
228 calculated by Hsu et al. [1990] for 24 December (their Figure 3) showed values greater than 50
229 W m^2 over South America and the tropical North Atlantic. Their 11-day mean 250 mb
230 streamfunction anomalies also displayed a wave train from the Indian to the Atlantic, along the
231 Northern Hemisphere, at the same day (their Figure 4). The wave pattern in the Southern
232 Hemisphere is not clear, but 5 days later, 29 December, a wave train seems more organized from
233 Indonesia to the East Pacific. The same wave train can be observed in Berbery and Nógues-
234 Paegle [1993] for the last pentad of December 1985 (their Figure 11). The upper-level wave train
235 displayed on Figure 4b,c apparently represents the link between the SPCZ and the SACZ as a
236 response to intraseasonal convective activity, in agreement with the modeling results by Grimm
237 and Silva Dias [1995].

238 5.2 *Independent SACZ*

239 Independent SACZ events are very common (64 events) but exhibit weaker anomalies
240 relative to the composite cycle of SACZ preceding MJO events (Figure 3f-j). The most striking
241 feature is the small amplitude of significant convective and pressure anomalies over the Eastern
242 Hemisphere tropics throughout the cycle suggesting little or no connection to intraseasonal
243 activity elsewhere.

Upper-level geopotential anomalies do not exhibit the same wave train evolution linking the warm pool to South America (Figure 4f-j). Moreover, the amplitude of the anomalies is generally smaller. Positive 200 mb geopotential anomalies are observed over southern South America accompanied by negative anomalies to the south at day -5 (Figure 4g). At composite day 0, the dipole of negative geopotential anomalies near 30°S and positive anomalies centered slightly north of 60°S is present as a result of SACZ convection.

Convective anomaly at day +5 for independent SACZ events exhibits slightly smaller horizontal extent and minimum OLR anomalies are generally 5 to 10 W m^{-2} weaker than the anomalies observed during SACZ events preceding the MJO (Figure 3). Overall, the magnitude and structure of global anomalies lead to a weaker independent SACZ.

6. Negative zonal stretching deformation and MJO-dependent SACZ events

Figure 5 display intraseasonal OLR composites observed at days 0 and +5 for both SACZ preceding MJO events (Figure 5a,b) and independent SACZ events (Figure 5c,d). Color shadings represent regions of unfiltered 200 mb zonal stretching deformation anomalies ($\partial \overline{U} / \partial x$). In the case of SACZ preceding the MJO, negative zonal stretching deformation anomalies are observed off the eastern coast of Brazil, coinciding with the extension of deep convection into the Atlantic Ocean (Figure 5c,d). For independent SACZ events, there is only a small, but significant, area of negative zonal stretching deformation over the same region. Although it seems that the anomalies are far more important during for SACZ events preceding the MJO, both cases support the idea of wave energy accumulation in the region, particularly over the oceanic portion of the SACZ.

The intraseasonal convective evolution of the two composite cycles at 15°S is given in Figure 6, together with filtered 3-6-day OLR and zonal stretching deformation data composited relative to the intraseasonal convective events. The time-longitude diagrams indicate that high frequency disturbances propagating equatorward are important for both SACZ categories, suggesting that

these synoptic systems are contributing to energy accumulation as highlighted by the convective and negative stretching deformation anomalies. In Figure 6a, the synoptic disturbance located at 60°W on day -6 has a nearly constant propagation speed of approximately 12 m s^{-1} until it reaches 40°W on day -4. On day 0, another system is observed just west of 50°W but its eastward propagation speed is reduced to 6 m s^{-1} during its propagation to 40°W. The same deceleration is noticed between 50°W and 40°W for the subsequent synoptic system. The shadings of zonal stretching deformation show the same behavior. The independent SACZ cycle also exhibits high frequency disturbances propagating to the east, but their OLR and the negative zonal stretching deformation anomalies are smaller in magnitude.

Using 3-6-day OLR minima below -1 standard deviation at 25°S, 45°W to identify synoptic disturbances in the core of the SACZ region, it is noted that from all 21 MJO-dependent SACZ, 19 occurred concurrently with a synoptic disturbance in the region. For independent SACZ events, 52 out of 64 cases occurred with the presence of a synoptic disturbance in the SACZ region. Composites of these synoptic systems reveal hints of the wave accumulation process in the vicinity of the SACZ at synoptic time scales (Figure 7). At day -2, an area of negative OLR anomalies is positioned just north of 30°S accompanied by a diagonal band of negative zonal stretching deformation ahead just before it enters the SACZ climatological domain. Negative OLR and zonal stretching deformation anomalies intensify as the system propagates northeastward along the coast, with negative stretching deformation leading OLR anomalies. At the same time, there is also a decrease in longitudinal wavelength most marked east of 40°W and as the system weakens in the second half of the high frequency cycle and propagation veers northward.

7. Summary and Conclusions

Intraseasonal associations between the MJO and the SACZ are often described in the literature with a focus on eastward propagation of MJO-related anomalies through the tropics

and extratropics favoring SACZ convection once the signals reach South America. Here, we demonstrate that, considering only relatively strong events (exceeding one standard deviation), it is more common to observe a strong SACZ preceding an MJO event. However, the occurrence of an intense SACZ before a MJO active phase over the Indian Ocean is a consequence of the MJO life cycle. The MJO active phase is intrinsically related to its preceding convective break, when a large-scale Rossby-Kelvin wave develops over the warm pool [Hirata et al., 2013]. The eastward propagation of MJO-related anomalies during a convective break interacts with the remnants of convection to its east and excites an extratropical wave train linking the South Pacific to South America. The wave spurs high-frequency synoptic disturbances to propagate equatorward into a region of climatological negative zonal stretching deformation that coincides with the climatological position of the SACZ.

At synoptic frequencies, a disturbance propagating northeastward into de SACZ core region longitudinally shrinks, slows down and intensifies while negative stretching deformation anomalies strengthens ahead, signaling wave energy accumulation. A similar behavior is observed in the SPCZ region [Widlansky et al., 2010]. In the Pacific, the region of climatological negative stretching deformation is caused by the zonal sea surface temperature gradient. Over South America, this region of zonal deceleration of upper-level winds is a result of the summertime establishment of the Bolivian High and the Nordeste Low system in the upper levels over the South Atlantic, explaining the marked seasonality of SACZ activity.

The SACZ events within the MJO cycle corresponds to approximately 20% of all identified SACZ events (21 out of 106) but are more intense and last longer than SACZs independent on the MJO (Figure 6). This relationship indicates that these MJO-dependent SACZ events are more predictable than the weaker, independent SACZs. Because intense and long-lasting SACZ events

317 are usually associated with extreme rainfall over heavily populated regions of southeastern Brazil
318 [Carvalho et al., 2002], it is possible that this information extends the range of SACZ-related
319 extreme precipitation events during the summer seasons. The observed life cycle differences
320 described here illustrate the dependency of intense, long-lasting SACZ events on extratropical
321 wave activity associated with the MJO cycle. Moreover, it is shown that synoptic wave energy
322 accumulation is instrumental in deepening convection and extending it over the Atlantic Ocean.
323 Although the fact that accumulation of wave energy acts to intensify some SACZ events related
324 to MJO signals, the triggering mechanism of most SACZs is still unclear and deserves further
325 investigation.

326 **References**

327 Berbery, E.H. and J. Nogués-Paegle (1993), Intraseasonal interactions between the tropics and
328 extratropics in the Southern Hemisphere, J. Atmos. Sci., 50, 1950-1965.

329 Carvalho, L.M.V., C. Jones, and B. Liebmann (2002), Extreme precipitation events in
330 southeastern South America and large-scale convective patterns in the South Atlantic
331 Convergence Zone, J. Clim., 15, 2377-2394.

332 Carvalho, L.M.V., C. Jones, and Brant Liebmann (2004), The South Atlantic Convergence Zone:
333 intensity, form, persistence, and relationship with intraseasonal to interannual activity and
334 extreme rainfall. J. Clim., 17, 88-108.

335 Chen, M., W. Shi, P. Xie, V.B.S. Silva, V.E. Kousky, R.W. Higgins, and J.E. Janowiak (2008),
336 Assessing objective techniques for gauge-based analyses of global daily precipitation, J.
337 Geophys. Res., 113, D04110, doi: 10.1029/2007JD009132.

Cunningham, C.A.C. and I.F.A. Cavalcanti (2006), Intraseasonal modes of variability affecting the South Atlantic Convergence Zone, Int. J. Clim., 26 (9), 1165-1180.

Grimm, A.M. and P.L. Silva Dias (1995), Analysis of tropical-extratropical interactions with influence functions of a barotropic model, J. Atmos. Sci., 52, 3538-3555.

Hirata, F., P.J. Webster, and V.E. Toma (2013), Distinct manifestation of austral summer intraseasonal oscillations, Geophys. Res. Lett., 40, doi: 10.1002/grl.50632.

Hsu, H.H., B.J. Hoskins, and F.F. Jin (1990), The 1985/86 intraseasonal oscillation and the role of the extratropics, J. Atmos. Sci., 47, 823-839.

Jones, C. and L.M.V. Carvalho (2002), Active and break phases in the South American monsoon system, J. Clim., 15, 905-914.

Kodama, Y. (1992), Large-scale common features of subtropical precipitation zones (the Baiu frontal zone, the SPCZ, and the SACZ) 1: characteristics of subtropical frontal zones, J. Meteorol. Soc. Japan, 70 (4), 813-836.

Lenters, J.D. and K.H. Cook (1997), On the origin of the Bolivian High and related circulation features of the South American climate, J. Atmos. Sci., 54, 656-678.

Liebmann, B., G.N. Kiladis, J.A. Marengo, T. Ambrizzi, and J.D. Glick (1999), Submonthly convective variability over South America and the South Atlantic Convergence Zone, J. Clim., 12, 1877-1891.

Liebmann, B. and C.A. Smith (1996), Description of a complete (interpolated) outgoing longwave radiation data set. Bull. Am. Meteorol. Soc., 77, 1275-1277.

Livezey, R.E. and W.Y. Chen (1983), Statistical field significance and its determination by Monte Carlo techniques, Mon. Wea. Rev., 111, 46-59.

Matthews, A.J., Propagation mechanisms for the Madden-Julian oscillation, Q.J.R. Meteorol. Soc., 126, 2637-2651.

Nieto-Ferreira, R., T.M. Rickenbach, and E.A. Wright (2011), The role of cold fronts in the onset of the monsoon season in the South Atlantic Convergence Zone, Q.J.R. Meteorol. Soc., 137, 908-922.

Nogués-Paegle, J. and K.C. Mo (1997), Alternating wet and dry conditions over South America during summer, Mon. Wea. Rev, 125, 279-291.

Nogués-Paegle, J., L.A. Byerle, and K.C. Mo (2000), Intraseasonal modulation of South American summer precipitation, Mon. Wea. Rev., 128, 837-850.

Robertson, A.W. and C.R. Mechoso (2000), Interannual and interdecadal variability of the South Atlantic convergence Zone, Mon. Wea. Rev., 128, 2947-2957.

Webster, P.J. and H.R. Chang (1997), Atmospheric wave propagation in heterogeneous flows: basic flow controls on tropical-extratropical interaction and equatorial wave modification. Dyn. Atmos. Oceans, 27, 722-733.

Widlansky, M., P.J. Webster, and C.D. Hoyos (2010), On the location and orientation of the South Pacific Convergence Zone, Clim. Dyn., 36, 561-578, doi: 10.1007/s00382-010-0871-6.

Tables

Table 1. Number of SACZ events and lead-lag relationships with intraseasonal events in the Eastern Hemisphere. Events are defined based on principal component time series exceeding 1 standard deviation. The lead is defined whenever one event is observed before another with 20 days in advance (at most). The time window is based on the lead-lag correlations in Figure 2 and extends to 20 days to account for lead-lag variations.

	Number of events	Average lag (days)
MJO leads SACZ	9	6
ED leads SACZ	3	9
SACZ leads MJO	**21**	9.5
SACZ leads ED	7	11
SACZ leads EI	2	4
Independent SACZ	**64**	-
Total number of SACZ events	106	-

Figures

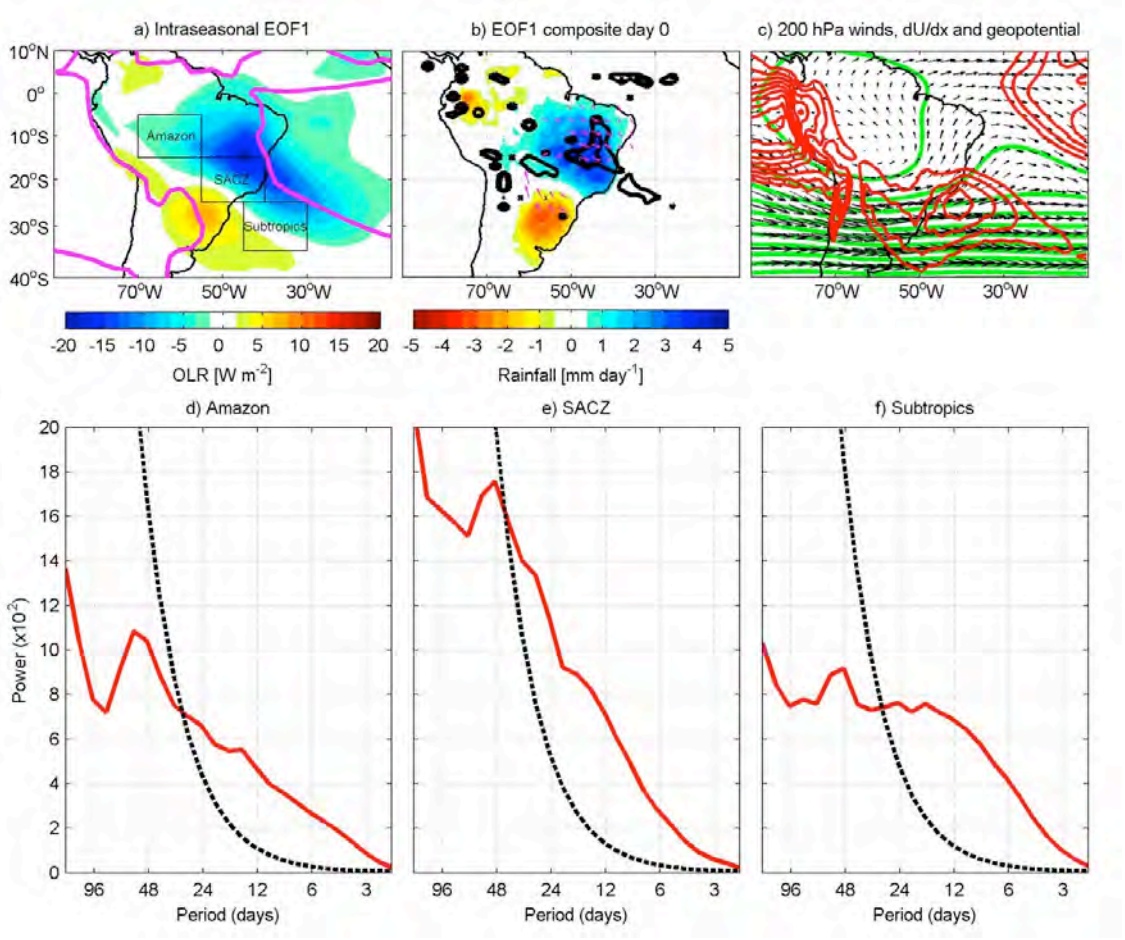

Figure 1. (a) First intraseasonal EOF for the domain. Magenta contour outlines the 245 W m^{-2} October-March mean OLR (1979-2011). The boxes indicate the areas used to calculate the spectra in d-f. (b) Composite day 0 relative to SACZ-PC1 events using CPC rainfall (shading) and ERA-Interim 850 mb winds (vectors) and negative 500 mb omega (black contours at -0.05 and -0.025 Pa s^{-1}), significant at 95%. (c) Mean October to March (1979-2011) ERA-Interim 200 mb winds, geopotential (green), and negative zonal stretching deformation (red). (d-f) Global wavelet spectra of unfiltered, area-averaged OLR taken from the boxes indicated in (a). The dashed line indicates the significance level based on 95% autocorrelation.

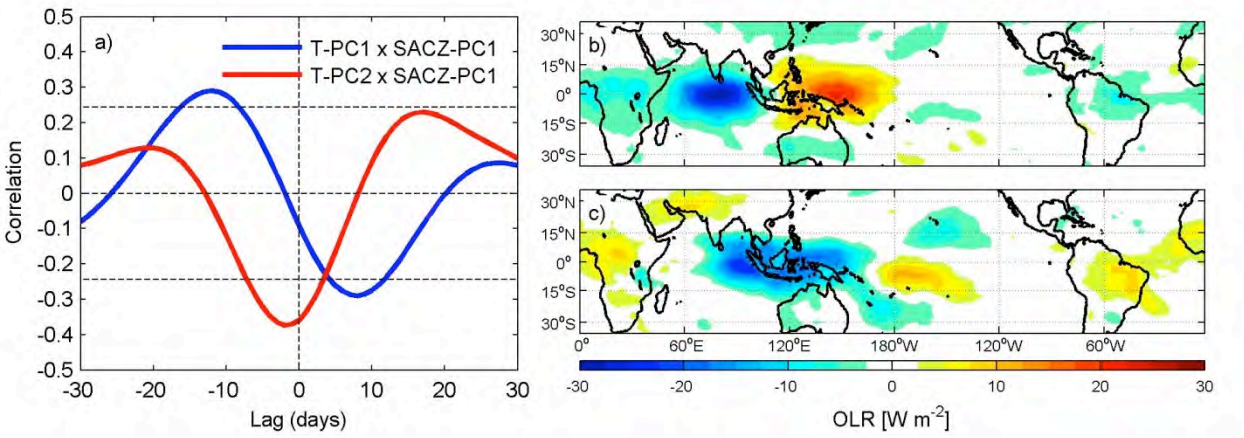

Figure 2. (a) Correlation between the first two PCs of tropical intraseasonal EOF modes from Hirata et al. [2013] (T-PC1 and T-PC2) and the SACZ-PC1. The dashed horizontal lines above (below) 0.2 (-0.2) indicates the 95% significance level calculated by a t-test using 4 degrees of freedom per season. (b,c) First and second tropical intraseasonal EOF modes from Hirata et al. [2013].

401

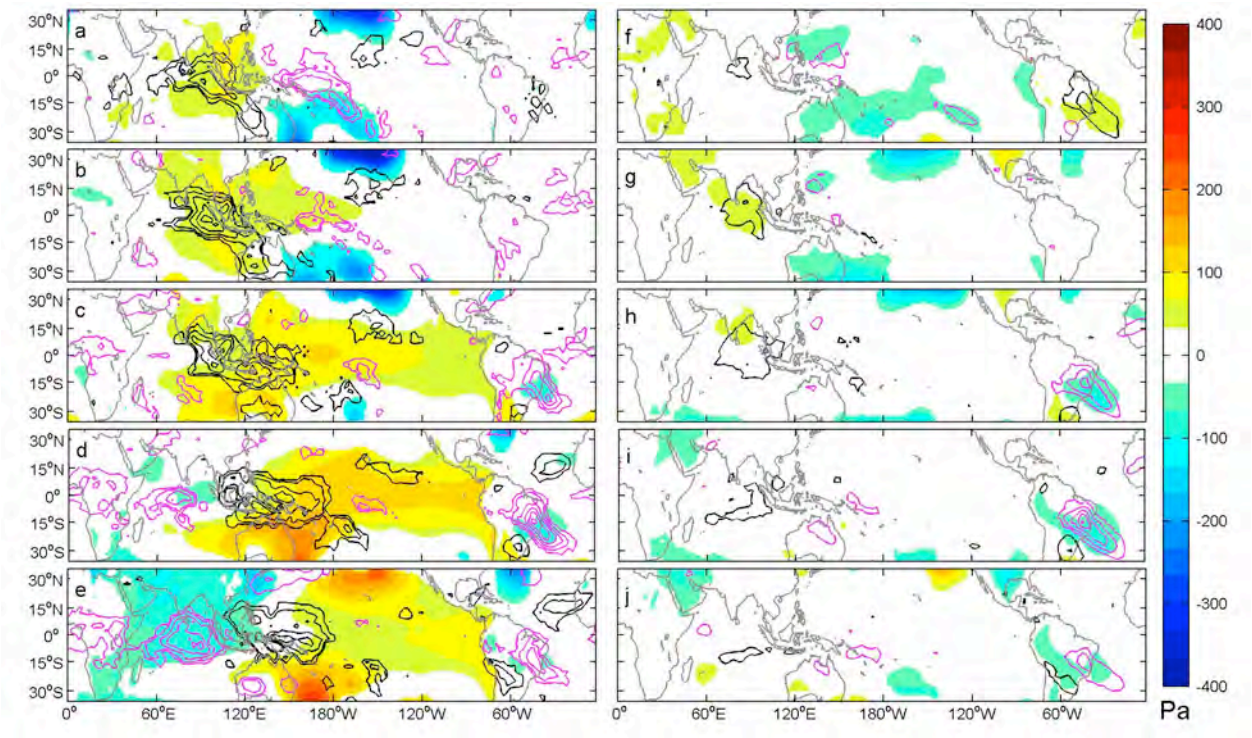

402

403 **Figure 3.** (a-e) OLR and surface pressure composites for days -10, -5, 0, +5, and +10 for MJO-
404 dependent SACZ events. (f-j) Same as (a,e) but for independent SACZ events. Shading denotes
405 surface pressure anomalies and black (magenta) contours represent OLR positive (negative)
406 anomalies (from -35 to 35 W m^{-2} at 5 W m^{-2} intervals, 0 line is omitted). Only values significant
407 at 95% are displayed.

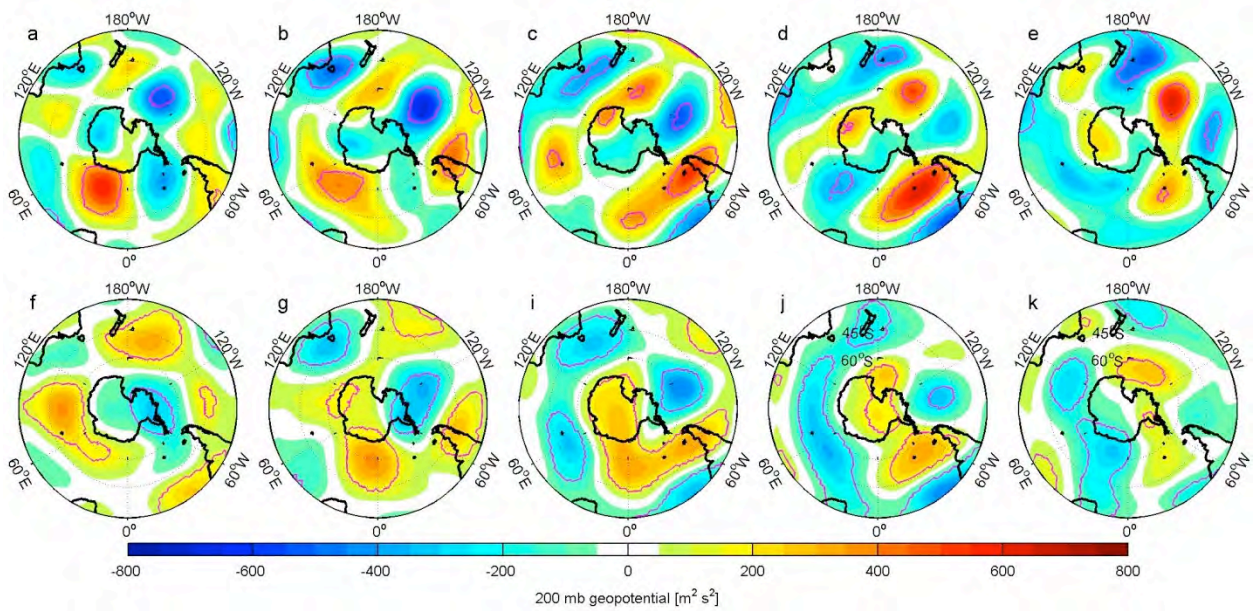

408

409 **Figure 4.** (a-e) 200 mb geopotential composites for days -10, -5, 0, +5, and +10 for MJO-

410 dependent SACZ events. (f-j) Same (a.e) but for independent SACZ events. Magenta contours

411 indicates 95% significance.

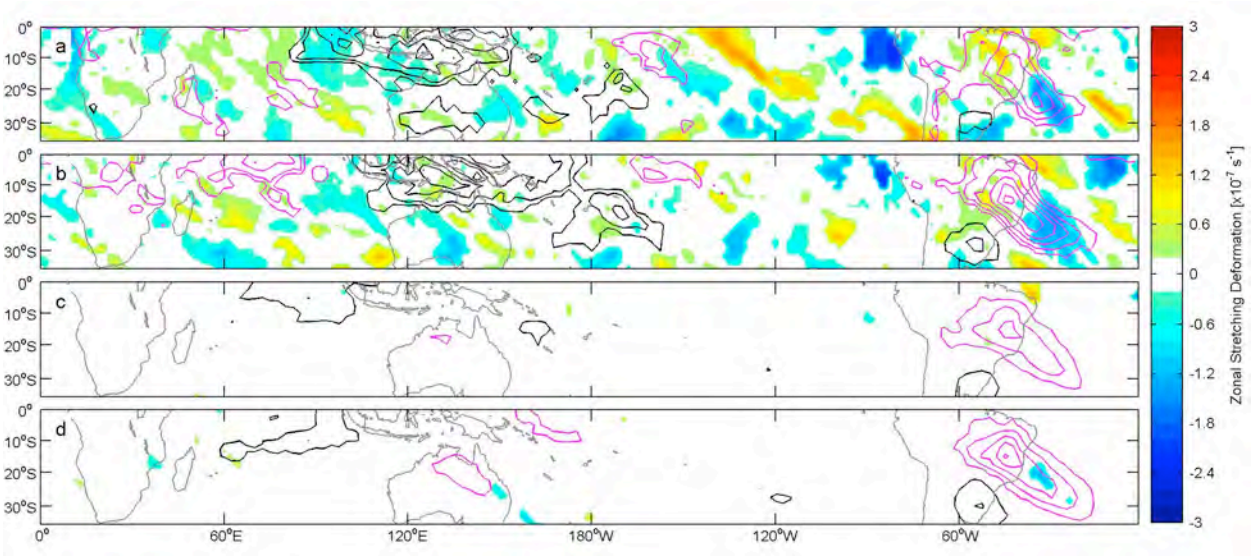

Figure 5. (a,b) OLR (contours) and zonal stretching deformation (shadings) composites for days 0 and +5 for MJO-dependent events. (c-d) Same as (a,b) but for independent SACZ events. OLR contours are the same as in Figure 3.

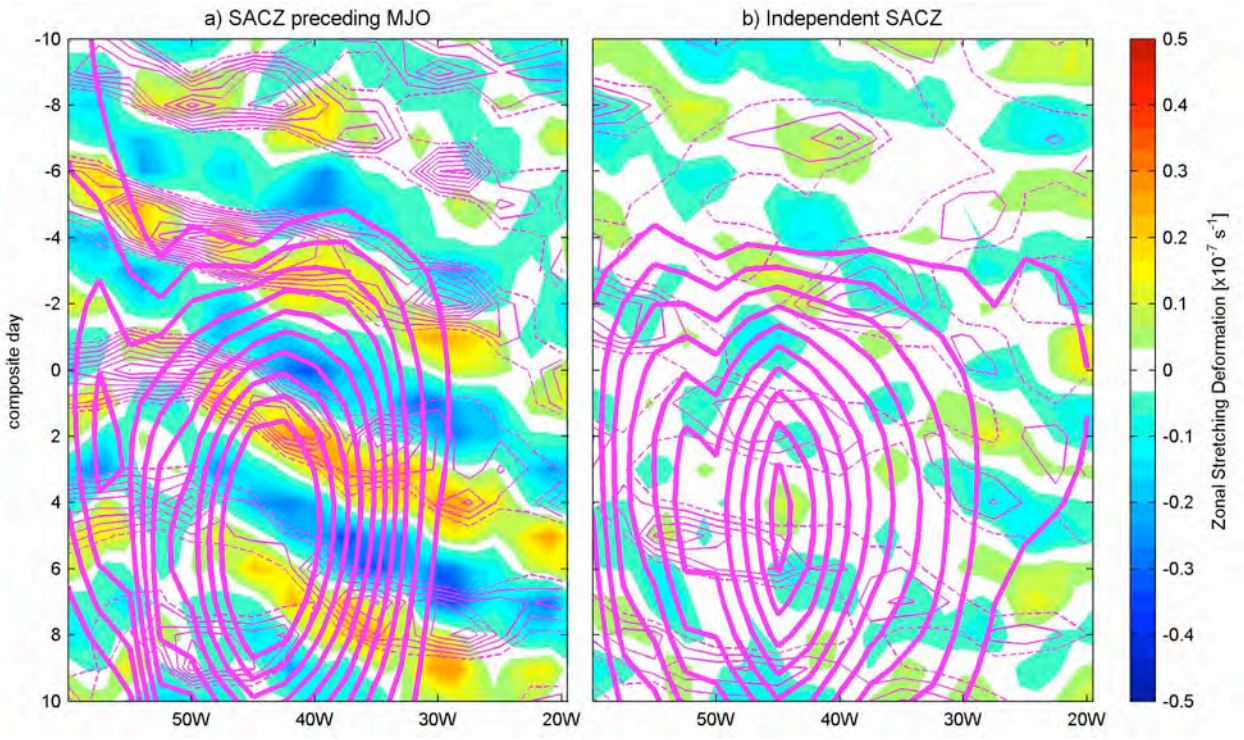

Figure 6. (a) Time-longitude diagram of negative intraseasonal OLR (thick magenta contour, from -25 to -5 W m^{-2} at 5 W m^{-2} intervals), synoptic OLR (thin magenta contours, from -10 to -1 W m^{-2} at 1 W m^{-2} intervals) with the dashed line indicating the zero contour), and synoptic zonal stretching deformation (shadings). (b) Same as (a) but for independent SACZ events.

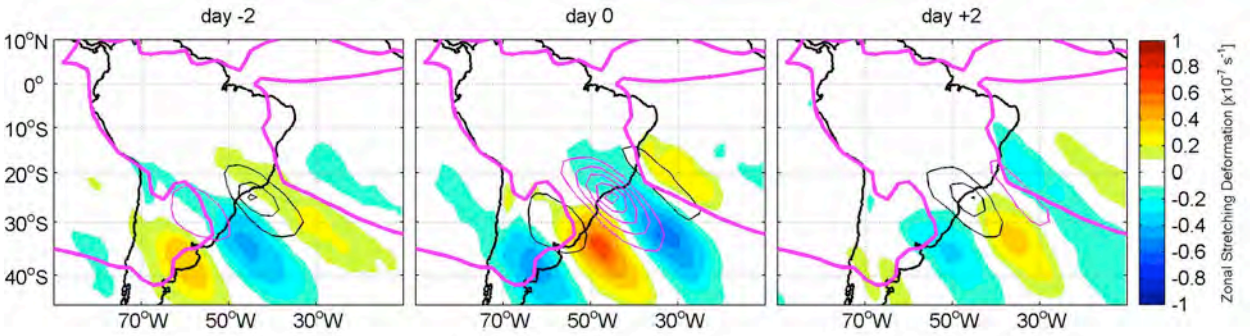

Figure 7. Synoptic OLR (thin contours) and zonal stretching deformation (shadings) composites for days -2, 0, and +2 with respect to 3-6-day minima OLR below -1 standard deviation at 25°S, 45°W. Black (magenta) contours represent positive (negative) OLR from -25 to -5 W m^{-2} at 5 W m^{-2} intervals. Thick magenta contour outlines the 245 W m^{-2} October to March (1979-2011) mean OLR.